Journal of Photochemistry and Photobiology A: Chemistry 199 (2008) 336–344

Contents lists available at ScienceDirect

Journal of Photochemistry and Photobiology A: Chemistry

journal homepage: www.elsevier.com/locate/jphotochem

The CH_3CO quantum yield in the 248 nm photolysis of acetone, methyl ethyl ketone, and biacetyl

B. Rajakumar[a,b,1], Tomasz Gierczak[a,b,2], Jonathan E. Flad[a,b,3], A.R. Ravishankara[a,4], James B. Burkholder[a,*]

[a] Earth System Research Laboratory, Chemical Sciences Division, National Oceanic and Atmospheric Administration, 325 Broadway, Boulder, CO 80305-3328, USA
[b] Cooperative Institute for Research in Environmental Sciences, University of Colorado, Boulder, CO 80309, USA

ARTICLE INFO

Article history:
Received 7 February 2008
Received in revised form 14 June 2008
Accepted 18 June 2008
Available online 28 June 2008

Keywords:
Acetyl radical
Acetone
Photolysis
Quantum yield

ABSTRACT

We report measurements of the CH_3CO quantum yield, Φ_{CH_3CO}, following the 248 nm pulsed laser photolysis of acetone ($CH_3C(O)CH_3$), methyl ethyl ketone ($CH_3C(O)CH_2CH_3$), and biacetyl ($CH_3C(O)C(O)CH_3$). CH_3CO quantum yields at 248 nm were measured at 296 K, relative to CH_3CO reference systems. CH_3CO was detected using cavity ring-down spectroscopy at wavelengths between 490 and 660 nm. Measurements were performed between 60 and 670 Torr (He, N_2 bath gases) and the obtained CH_3CO quantum yields in the low-pressure limit, $\Phi^0_{CH_3CO}$, were 0.535 ± 0.09, 0.41 ± 0.08, and 0.76 ± 0.11, for acetone, methyl ethyl ketone, and biacetyl, respectively. The quoted uncertainties are 2σ (95% confidence level) and include estimated systematic errors. An increase in Φ_{CH_3CO} with increasing bath gas pressure, which depended on the identity of the collision partner (He, N_2), was observed. The present results are compared with previous quantum yield determinations.

Published by Elsevier B.V.

1. Introduction

The photochemistry of acetone has been extensively studied both experimentally and theoretically over the past several decades [1]. The interest in the photodissociation of acetone for atmospheric purposes arises because it can be a significant source of HO_x ($OH + HO_2$) in the upper troposphere [2]. The rate for the photolytic loss of acetone in the atmosphere is calculated from the product of its UV absorption cross-section, photolysis quantum yield, $\Phi_{Acetone}$, and the solar flux. Of these parameters, the acetone photolysis quantum yield (including its wavelength, pressure and temperature dependence) in the actinic region, $\lambda > 290$ nm, is the least-well characterized. Acetone photodissociates through two channels over the wavelength region of atmospheric interest

$$CH_3C(O)CH_3 + h\nu \rightarrow CH_3CO + CH_3, \quad \lambda_T = 338\,\text{nm} \tag{1a}$$

$$CH_3C(O)CH_3 + h\nu \rightarrow 2CH_3 + CO, \quad \lambda_T = 298\,\text{nm} \tag{1b}$$

where λ_T is the photolysis threshold at 298 K calculated from standard heats of formation [3,4]. The absolute yields for these two dissociation channels and the collisional quenching of electronically excited acetone play an important role in determining the formation of PAN ($CH_3C(O)O_2NO_2$), the extent of formation of HO_x, and loss of acetone in the atmosphere. PAN is a reservoir for NO_x ($NO + NO_2$) and is formed via the reactions

$$CH_3CO + O_2 + M \rightarrow CH_3C(O)O_2 + M \tag{2}$$

$$CH_3C(O)O_2 + NO_2 + M \leftrightarrow CH_3C(O)O_2NO_2 + M \tag{3}$$

Therefore, knowledge of the acetone quantum yield (loss of acetone) and the branching ratio for channels (1a) and (1b), as a function of wavelength, pressure, and temperature, is important for atmospheric modeling. Direct quantum yield measurements in the wavelength range most important to the atmosphere, $\lambda > 290$ nm, are difficult due to the weak absorption by acetone in this wavelength region. Therefore, the quantum yields at longer wavelengths are often measured relative to that at shorter wavelengths. Knowledge of the photolysis quantum yields at the shorter wavelengths also helps build our general understanding of the photodissociation of acetone.

Previous acetone photolysis studies have primarily relied on indirect experimental methods to determine the loss of acetone [5,6], the formation of reaction products generated by secondary

* Corresponding author. Tel.: +1 303 497 3252; fax: +1 303 497 5822.
E-mail address: James.B.Burkholder@noaa.gov (J.B. Burkholder).
[1] Current address: Department of Chemistry, Indian Institute of Technology, Madras 600036, India.
[2] Permanent address: Department of Chemistry, Warsaw University, ul. Zwirki i Wigury 101, 02-089 Warsaw, Poland.
[3] Current address: The Ohio State University, Agricultural Technical Institute, Wooster, OH 44691, USA.
[4] Also associated with the Department of Chemistry and Biochemistry, University of Colorado, Boulder, CO 80309, USA.

1010-6030/$ – see front matter. Published by Elsevier B.V.
doi:10.1016/j.jphotochem.2008.06.015

chemistry of the primary photoproducts [1,7], and/or the formation of stable end-products [5,8–11]. Recent studies have monitored the primary photolysis product CO [12] as well as CH_3 and CH_3CO, [13] formed in the 248 nm pulsed laser photolysis of acetone, by using infrared and UV absorption methods, respectively. The current knowledge for the photochemistry of acetone at 248 nm can be summarized as follows: (1) $\Phi_{Acetone}$ is near unity, within ~10%, and independent of bath gas pressure [5,6], (2) the acetone fluorescence quantum yield is negligible, <0.001 [14] and (3) the branching ratios for channels (1a) and (1b) are pressure dependent with Φ_{CH_3CO} increasing and Φ_{CO} decreasing at higher pressures [12,13]. However, there are discrepancies among the measured quantum yields that have significant implications for the interpretation of laboratory and atmospheric modeling studies.

Here, we report measurements of the CH_3CO quantum yield, Φ_{CH_3CO}, in the 248 nm photolysis of acetone at 296 K at total pressures in the range 60–670 Torr (He, N_2 bath gases). In addition, we have measured Φ_{CH_3CO} for the 248 nm photolysis of methyl ethyl ketone (MEK) and biacetyl (compounds that also contain the acetyl group)

$$CH_3C(O)CH_2CH_3 + h\nu \rightarrow CH_3CO + CH_3CH_2, \quad \lambda_T = 342\,nm \quad (4a)$$

$$CH_3C(O)CH_2CH_3 + h\nu \rightarrow CH_3 + CH_3CH_2CO, \quad \lambda_T = 323\,nm \quad (4b)$$

$$CH_3C(O)CH_2CH_3 + h\nu \rightarrow CH_3 + CO + CH_3CH_2, \quad \lambda_T = 302\,nm \quad (4c)$$

$$CH_3C(O)C(O)CH_3 + h\nu \rightarrow 2CH_3CO, \quad \lambda_T = 390\,nm \quad (5a)$$

$$CH_3C(O)C(O)CH_3 + h\nu \rightarrow CH_3CO + CO + CH_3, \quad \lambda_T = 338\,nm \quad (5b)$$

$$CH_3C(O)C(O)CH_3 + h\nu \rightarrow 2CH_3 + 2CO, \quad \lambda_T = 300\,nm \quad (5c)$$

The photochemistry of methyl ethyl ketone and biacetyl are of interest unto themselves and measurements of acetyl radical quantum yields are also useful to further our understanding of the UV photolysis of ketones in general. The present results are discussed in light of previously published studies.

2. Experimental details

The quantum yield for CH_3CO formation, Φ_{CH_3CO}, in the 248 nm pulsed laser photolysis of acetone, MEK, and biacetyl were determined relative to a known source of CH_3CO and relative to each another (as described in our previous study of the visible absorption spectrum of the CH_3CO radical [15]). Determining photolysis quantum yields using a relative method instead of an absolute method is advantageous because it eliminates the need to quantify both the absolute CH_3CO radical concentrations and the photolysis laser fluence. The relative method therefore improves the precision and accuracy of the quantum yield measurements by reducing contributions from possible systematic errors that are common to both the reference and sample measurements. In this study, CH_3CO quantum yields were measured relative to CH_3CO produced in the gas-phase reaction

$$OH + CH_3C(O)H \rightarrow H_2O + CH_3CO, \quad \Delta_r H = -29.4\,kcal\,mol^{-1} \quad (6a)$$

$$OH + CH_3C(O)H \rightarrow H_2O + CH_2C(O)H, \quad \Delta_r H = -24.5\,kcal\,mol^{-1} \quad (6b)$$

where $k_6(298\,K) = 1.4 \times 10^{-11}\,cm^3\,molecule^{-1}\,s^{-1}$ [3] and the CH_3CO product yield has been measured experimentally to be near unity, $0.95^{+0.017}_{-0.024}$ [16,17]. OH radicals were produced by the 248 nm pulsed laser photolysis of H_2O_2 or an O_3/H_2O/He mixture. CH_3CO was monitored using cavity ring-down spectroscopy (CRDS) [15].

The CH_3CO yield following the 248 nm pulsed laser photolysis of acetone is given by the following relationship

$$[CH_3CO]_0^{Acetone} = [Acetone] \times \sigma_{Acetone}(248\,nm) \times \Phi_{CH_3CO}(Acetone) \times F \quad (7)$$

where $[CH_3CO]_0^{Acetone}$ is the CH_3CO concentration produced from the photodissociation of acetone by the photolysis laser, $\sigma_{Acetone}(248\,nm)$ is the absorption cross-section ($cm^2\,molecule^{-1}$) of acetone at 248 nm, and F is the photolysis laser fluence (photon cm^{-2} $pulse^{-1}$). In Eq. (7), we have used acetone as the photolyte but analogous relationships also apply for MEK and biacetyl. For CH_3CO produced via the reference reaction, the concentration of CH_3CO radicals produced is given by

$$[CH_3CO]_0^{Ref} = [Ref] \times \sigma_{Ref}(248\,nm) \times F \times Y_{CH_3CO}(Ref) \quad (8)$$

where Ref is the OH precursor photolyte (either H_2O_2 or O_3 in our experiments) and $Y_{CH_3CO}(Ref)$ is the overall yield of CH_3CO from the source chemistry, $Y_{CH_3CO}(H_2O_2) = 1.9$ and $Y_{CH_3CO}(O_3) = 1.71$, which is described in more detail later.

Combining Eq. (7) and Eq. (8) yields

$$\Phi_{CH_3CO}(Acetone) = \frac{[CH_3CO]_0^{Acetone}}{[CH_3CO]_0^{Ref}} \times \frac{[Ref]}{[Acetone]} \times \frac{\sigma_{Ref}(248\,nm)}{\sigma_{Acetone}(248\,nm)} \times Y_{CH_3CO}(Ref) \quad (9)$$

and illustrates the advantage of using a relative quantum yield measurement method. In Eq. (9), the photolysis laser fluence has canceled and $\Phi_{CH_3CO}(Acetone)$ is obtained from the ratio of the measured CH_3CO and precursor concentrations combined with well-known absorption cross-sections and source chemistry. Experimentally, the absorption coefficient, α_0 (described below), which is proportional to $[CH_3CO]_0$ was measured using CRDS (i.e., measurement of the absolute radical concentration is not needed). Expressing Eq. (9) in terms of the experimentally measured quantities yields

$$\Phi_{CH_3CO}(Acetone) = \frac{\alpha_0^{Acetone}}{\alpha_0^{Ref}} \times \frac{A_{Ref}}{A_{Acetone}} \times \frac{\sigma_{Acetone}(185\,nm)}{\sigma_{Ref}(\lambda_{Ref})} \times \frac{\sigma_{Ref}(248\,nm)}{\sigma_{Acetone}(248\,nm)} \times Y_{CH_3CO}(Ref) \quad (10)$$

where A_{Ref} and $A_{Acetone}$ are the measured UV absorptions for the reference compound and acetone at wavelengths λ_{Ref} (184.9 or 253.7 nm) and 184.9 nm, respectively. Table 1 lists the absorption cross-sections used in the data analysis.

The experimental apparatus used in this study consisted of a cavity ring-down spectroscopy (CRDS) setup coupled to a pulsed laser photolysis flow reactor as shown in Fig. 1. The pulsed CRDS probe beam and the pulsed excimer laser photolysis beam cross at a right angle. Details of the cavity ring-down technique are available elsewhere [18–21] and are only briefly described here. The details of this experimental apparatus have also been described in our recent study of the CH_3CO visible absorption spectrum [15]. The following sections provide a description of the CRDS apparatus and data analysis, the CH_3CO reference chemistry, and experimental details used in the present study.

Table 1
Summary of absorption cross-sections

Molecule	Wavelength (nm)	Cross-section (cm^2 $molecule^{-1}$)[a]	Reference
H_2O_2	214	3.30×10^{-19}	Sander et al. [3]
	248	8.20×10^{-20}	Sander et al. [3]
O_3	248	1.08×10^{-17}	Sander et al. [3]
	254	1.15×10^{-17}	Sander et al. [3]
	532	2.78×10^{-21}	Burkholder and Talukdar [30]
Acetaldehyde ($CH_3C(O)H$)	248	9.73×10^{-21}	Martinez et al. [31]
	254	1.50×10^{-20}	Martinez et al. [31]
Acetone ($CH_3C(O)CH_3$)	184.9	2.91×10^{-18}	This work
	248	2.20×10^{-20}	Gierczak et al. [5]
	254	3.01×10^{-20}	Gierczak et al. [5]
Methyl ethyl ketone (MEK; $CH_3C(O)CH_2CH_3$)	184.9	1.31×10^{-18}	This work
	248	2.17×10^{-20}	Martinez et al. [31]
Biacetyl ($CH_3C(O)C(O)CH_3$)	184.9	1.46×10^{-18}	This work
	248	3.05×10^{-20}	Horowitz et al. [32]

[a] The uncertainties in the quoted cross-sections are best obtained from the error analyses given in the cited references.

2.1. Crossed pulsed laser photolysis—cavity ring-down spectroscopy

The cavity ring-down time constant, τ, is related to the absorption coefficient, $\alpha(\lambda)$ (cm^{-1}), by the relationship

$$\alpha(\lambda) = [CH_3CO] \times \sigma_{CH_3CO}(\lambda) = \frac{1}{c} \times \frac{d}{L_s} \times \left(\frac{1}{\tau(\lambda)} - \frac{1}{\tau_0(\lambda)} \right) \quad (11)$$

where λ is the wavelength of the CRDS probe beam, $\sigma_{CH_3CO}(\lambda)$ is the absorption cross-section (cm^2 $molecule^{-1}$) of CH_3CO at wavelength λ, d is the cavity pathlength (cm), L_s is the pathlength (cm) for the absorbing sample, c is the speed of light, and $\tau(\lambda)$ and $\tau_0(\lambda)$ are the ring-down time constants (s) with and without the absorber present, respectively. The CRDS probe beam was taken from a frequency doubled Nd:YAG laser (532 nm) or a 308 nm excimer pumped dye laser (wavelengths in the range 490–660 nm were used). Light exiting the rear mirror of the optical cavity was collected with a fiber optic and detected using a photomultiplier tube. Signals were collected and averaged on a 16-bit waveform digitizer at a sample rate of 1 MHz. The wavelength of the dye laser output was measured using a laser wavelength meter. Quantum yields were measured using CRDS probe wavelengths between 490 and 660 nm, the same range used in our previous CH_3CO absorption spectrum measurements [15]. Using a range of probe beam wavelengths required using several sets of CRDS mirrors with τ_0 values in the range 60–120 μs for a cavity length of 1 m.

The laser photolysis beam passed through the reaction cell at a right angle to the CRDS optical cavity. The reactor, which was mounted midway between the CRDS mirrors, was a 25 cm long 5 cm diameter Pyrex tube with 248 nm AR coated windows and side-arms to allow the CRD beam to pass through its center. This configuration enabled CH_3CO to be produced directly in the CRD optical path. Gas mixtures flowed the length of the reactor. The CRD pathlength, L_s, for the absorbing species was 4.7 cm. The 248 nm excimer laser photolysis beam was monitored continuously with a calibrated power meter mounted outside the exit window of the reactor.

2.2. CH_3CO reference chemistry

In the reference system, CH_3CO radicals were produced following the 248 nm pulsed laser photolysis of either H_2O_2 or an

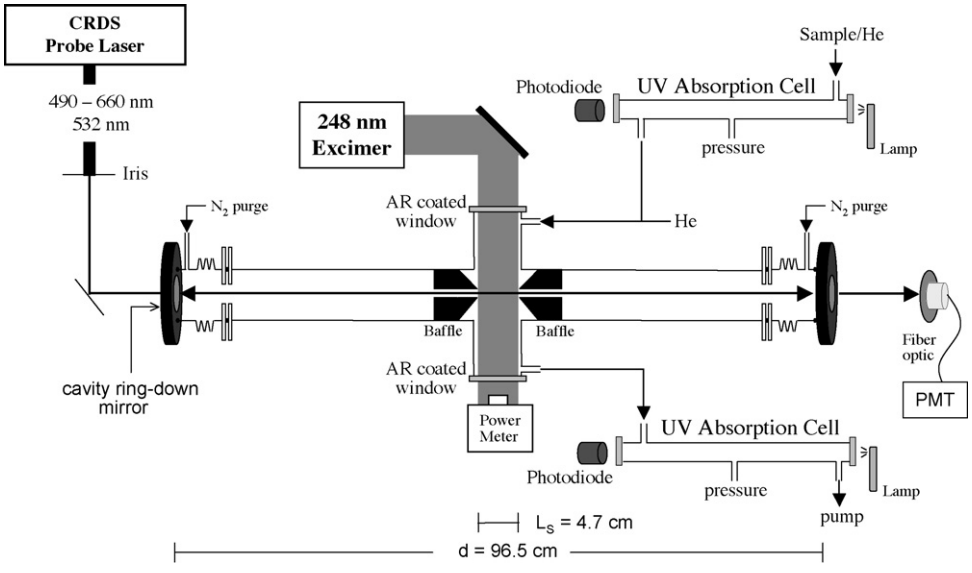

Fig. 1. Schematic of the crossed pulsed laser photolysis—cavity ring-down apparatus.

O_3/H_2O/He mixture to produce OH radicals

$$H_2O_2 + h\nu \rightarrow 2OH \quad (12)$$

or

$$O_3 + h\nu \rightarrow O(^1D) + O_2(^1\Delta) \quad (13a)$$

$$O_3 + h\nu \rightarrow O(^3P) + O_2(^3\Sigma) \quad (13b)$$

$$O(^1D) + H_2O \rightarrow 2OH \quad (14)$$

in the presence of an excess of acetaldehyde. The reaction of OH with acetaldehyde

$$OH + CH_3C(O)H \rightarrow H_2O + CH_3CO \quad (6a)$$

produced a stoichiometric amount of CH_3CO. OH radicals were produced instantaneously as a primary photolysis product when H_2O_2 was used. OH was rapidly consumed to produce CH_3CO via reaction (6a) within 20 μs. When O_3 photolysis was used, OH was produced via the rapid reaction of $O(^1D)$ with H_2O. A high concentration of H_2O, ~5 Torr, was used to ensure complete and rapid scavenging of $O(^1D)$, $k_{14}(298\,K) = 2 \times 10^{-10}$ cm^3 molecule^{-1} s^{-1} [3]. The quantum yield for $O(^1D)$ formation in reaction (13a) and (13b) is 0.9 [3]. The reaction of the $O(^3P)$ atoms, which are produced in reaction (13b), with $CH_3C(O)H$

$$O(^3P) + CH_3C(O)H \rightarrow OH + CH_3CO \quad (15)$$

occurs on a longer time scale than reaction (6a) and (6b), $k_{15}(298\,K) = 4.5 \times 10^{-13}$ cm^3 molecule^{-1} s^{-1} [3]. Reaction (15) leads to the direct formation of an CH_3CO radical and an additional CH_3CO radical via the subsequent reaction of the OH radical with $CH_3C(O)H$. This slower secondary radical chemistry did not significantly influence the determination of Φ_{CH_3CO} as will be shown in Section 3. For both OH radical sources, the CH_3CO absorption coefficient at time zero, α_0, was obtained by extrapolating the measured change in α in time to $t = 0$. The first-order rate coefficient for the loss of CH_3CO under these conditions was measured directly and was typically ~400 s^{-1} (i.e., the CH_3CO concentration did not change rapidly on the time scale of the measurements and the extrapolation to $t = 0$ did not contribute significantly to the uncertainty in the determination of α_0). The photolysis laser fluence and precursor concentrations were varied during the course of this study resulting in $[CH_3CO]_0$ values in the range $(1–6) \times 10^{12}$ molecule cm^{-3}.

2.3. CH_3CO quantum yield determinations

Φ_{CH_3CO} was determined in a series of back-to-back measurements that included the pulsed laser photolysis of acetone, MEK, or biacetyl and the measurement of CH_3CO produced in one or both of the reference systems. Performing experiments in a back-to-back sequence enabled the photolysis laser fluence and other experimental parameters (such as gas flows and pressures) to be held nearly constant during the Φ_{CH_3CO} determination. The majority of our experiments were performed using a CRD probe wavelength of 532 nm, although, some experiments were also performed using wavelengths, over the range 490–660 nm [15]. Experiments performed using 490–660 nm yielded Φ_{CH_3CO} values in very good agreement, within 8%, with those measured using 532 nm.

The concentrations of H_2O_2, O_3, acetone, MEK, and biacetyl used in Eq. (10) were measured on-line by UV absorption. UV absorption measurements were made using a Hg pen-ray lamp light source at 184.9 or 253.7 nm combined with narrow bandpass filters and a photodiode detector. Pyrex absorption cells, 1 in. diameter with quartz windows, with absorption pathlengths of 10, 25, 50, and 100 cm were used during the study. The absorption cell pathlength used depended on the compound and its concentration. The concentrations within the reactor were calculated from the absorption measurements and were scaled to make small corrections for flow dilution and differences in pressure between the absorption cells and the reactor. In some cases, the O_3 concentration was measured via its absorption in the Chappius band directly in the reactor using the CRD measurements.

2.4. Materials

He (UHP, 99.999%) and N_2 (UHP, >99.99%) were used as bath gases. Samples of acetone (>99.9%), methyl ethyl ketone ($CH_3C(O)CH_2CH_3$, >99%), biacetyl ($CH_3C(O)C(O)CH_3$, >99%), and acetaldehyde ($CH_3C(O)H$, >99.5%) were degassed using several freeze-pump–thaw cycles prior to use and stored under vacuum in Pyrex reservoirs with Teflon stopcocks. Samples were introduced into the gas flow by passing a flow of bath gas over the surface of the liquid prior to dilution with the main gas flow. The sample reservoirs were kept in constant temperature baths to help stabilize the sample flow. Concentrated H_2O_2 (>95%, as determined by titration with a standard $KMnO_4$ solution) was prepared by bubbling N_2 through a H_2O_2 sample, initially at ~60 wt%, for several days prior to use. H_2O_2 was introduced to the gas flow by bubbling a small flow of He through the liquid H_2O_2 sample. Ozone was prepared by passing O_2 (UHP, >99.99%) through a commercial ozonizer and stored on silica gel at 195 K. A dilute mixture of O_3 in He (~0.1% mole fraction) was prepared from this sample in a darkened 12 L Pyrex bulb. Flow from the bulb or a flow of He through the ozone silica gel trap were used to introduce ozone into the main gas flow.

Gas flow rates were measured using calibrated electronic mass flow meters. The total gas flow rate through the photolysis reactor was ~2500 sccm at 60 Torr total pressure. To ensure that a fresh sample was present for each photolysis laser pulse, experiments were performed with a laser repetition rate of 3 Hz. Pressures were measured using 100 and 1000 Torr capacitance manometers. All experiments were performed at ambient temperature, 296 ± 2 K.

3. Results and discussion

Initially, experiments were performed to test the linearity of the measured CH_3CO signal, α_0, with the photolyte concentration and the 248 nm photolysis laser fluence. Fig. 2 shows measured α_0 values, obtained for a range of acetone, MEK, and biacetyl concentrations, while the total pressure and photolysis laser fluence were held constant. In these experiments, the initial CH_3CO radical concentration increased as the ketone concentration was increased and the highest CH_3CO concentration obtained was $\sim 3 \times 10^{13}$ molecule cm^{-3}. For CH_3CO concentrations greater than $\sim 8 \times 10^{12}$ molecule cm^{-3} the observed ring-down profiles deviated from a single exponential decay due to the loss of CH_3CO on the same time scale as the ring-down measurement. The CH_3CO loss is most likely due to the reactions

$$CH_3CO + CH_3 \rightarrow \text{Products} \quad (16)$$

$$CH_3CO + CH_3CO \rightarrow \text{Products} \quad (17)$$

where $k_{16}(298\,K) = 1.43 \times 10^{-10}$ cm^3 molecule^{-1} s^{-1} [22] and $k_{17}(298\,K) = 1.8 \times 10^{-11}$ cm^3 molecule^{-1} s^{-1} [23]. Under conditions where the ring-down decay was not well represented by a single exponential, the ring-down profiles were analyzed using the simultaneous kinetics and ring-down (SKaR) method (approximating CH_3CO loss as first-order, which fit the measured ring-down profiles within the precision of the measurement) to determine α_0 [18]. Linearity between α_0 and the ketone concentration was observed for α_0 values up to 4×10^{-6} cm^{-1}. The majority

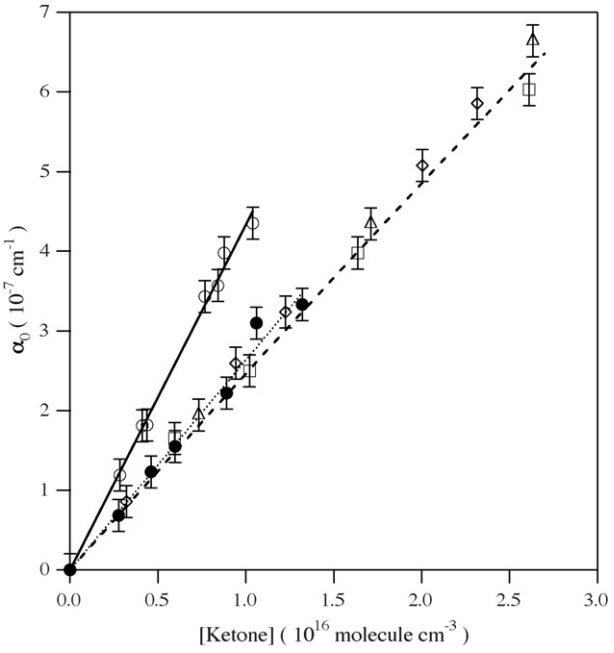

Fig. 2. Absorption coefficient, α_0, measured by cavity ring-down spectroscopy (CRDS) at 532 nm following the 248 nm pulsed laser photolysis of acetone (○; solid line), methyl ethyl ketone (MEK) (●; dotted line), and biacetyl (◊, △ and □; dashed line) vs. [ketone]. Measurements made for a given ketone were performed using constant photolysis laser fluence. The error bars are the absolute accuracy of the absorption coefficient measurement, 2×10^{-8} cm^{-1}. Measurements for biacetyl were made with 50 Torr (◊), 210 Torr (△) and 405 Torr (□) (N_2). The lines shown are linear least-squares fits to the data that illustrate the linear dependence of α_0 on the photolyte concentration.

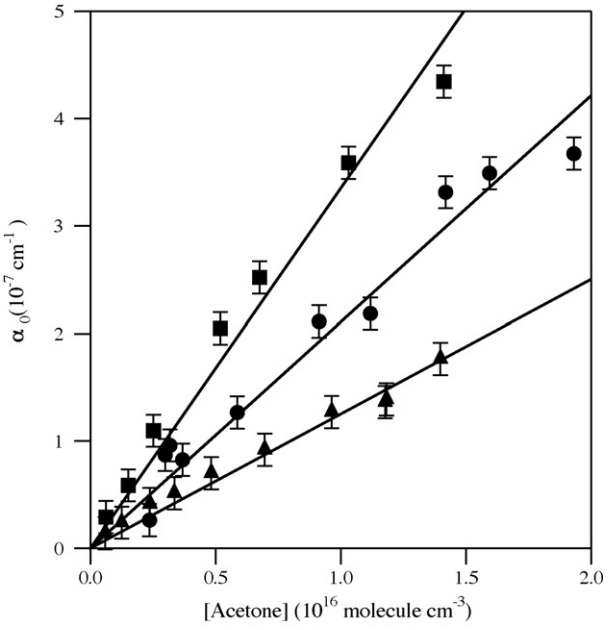

Fig. 3. Dependence of the absorption coefficient, α_0, measured by cavity ring-down spectroscopy (CRDS) at 532 nm following the 248 nm pulsed laser photolysis of acetone on the photolysis laser fluence. The photolysis laser fluences used were: 17.6 mJ cm^{-2} pulse^{-1} (■), 11.0 mJ cm^{-2} pulse^{-1} (●), and 6.5 mJ cm^{-2} pulse^{-1} (▲). The solid lines are linear least-squares fits to the data.

of the quantum yield experiments presented in this work were performed under conditions such that α_0 was $<0.7 \times 10^{-6}$ cm^{-1}, $[CH_3CO]_0$ $<6 \times 10^{12}$ molecule cm^{-3}, and the measured ring-down profiles were single exponential and α_0 was determined using Eq. (11). As shown in Fig. 2, α_0 was observed to vary linearly with the photolyte concentration over the range of concentrations used for our quantum yield measurements.

Fig. 3 shows results from a series of photolysis experiments performed with acetone as the photolyte for three different photolysis laser fluences. As shown in Fig. 2, α_0 increased linearly with increasing acetone concentration for each of the laser fluences used. The relative slopes, α_0 versus acetone concentration, are in good agreement with the ratios of the photolysis laser fluences, to within 5%. A similar level of linearity was also observed for MEK and biacetyl. The laser fluences used for the data shown in Fig. 3 includes the range of values used in the CH_3CO quantum yield experiments and demonstrates the linearity of the CH_3CO signal with photolysis laser fluence, Eq. (11).

CH_3CO quantum yields were measured at total pressures in the range 60–670 Torr with He and N_2 used as bath gases. CH_3CO quantum yields at 60 Torr were measured by reference to the calibration standards described in Section 2. The dependence of Φ_{CH_3CO} on pressure and collision partner (He or N_2) was determined relative to the values measured at 60 Torr total pressure. The results of our quantum yield measurements are summarized in Tables 2 and 3 and shown in Fig. 4. An average of the quantum yield, Φ_{CH_3CO}, values measured at 60 Torr are 0.60 ± 0.05, 0.51 ± 0.05, and 0.76 ± 0.07 for acetone, MEK, and biacetyl, respectively, where the quoted errors are the 2σ precision of the measurements. The quantum yields at 60 Torr were independent of bath gas, within the precision of the measurements. The Φ_{CH_3CO} values obtained using H_2O_2 as the OH source, agreed to within 10%, with those obtained using the O_3/H_2O source. This level of agreement indicates that no significant systematic errors were introduced in the measurements due to secondary source chemistry. The relative Φ_{CH_3CO} values for acetone, MEK, and biacetyl obtained in the back-to-back experiments were found in good agreement, within 5%, with the measurements made using the calibration standards. The overall uncertainty in the quantum yield values is discussed in Section 3.1.

Fig. 4 summarizes the results for the pressure dependent quantum yield values given in Tables 2 and 3 for He and N_2 bath gases. Due to the small change in Φ_{CH_3CO} with pressure, these experiments were performed in a series of back-to-back measurements

Table 2
Summary of CH_3CO quantum yield results in the 248 nm photolysis of acetone, biacetyl and methyl ethyl ketone with N_2 bath gas from this work at 296 K[a]

Acetone ($CH_3C(O)CH_3$)		Biacetyl ($CH_3C(O)C(O)CH_3$)		Methyl ethyl ketone ($CH_3C(O)CH_2CH_3$)	
Pressure (Torr)	Quantum yield	Pressure (Torr)	Quantum yield	Pressure (Torr)	Quantum yield
60	0.60	61	0.76	60	0.51
102	0.64	101	0.79	100	0.55
212	0.65	207	0.79	205	0.62
305	0.69	302	0.86	305	0.71
404	0.80	419	0.94	412	0.73
501	0.79	419	0.90	515	0.79
592	0.87	509	0.87	606	0.94
–	–	643	0.96	631	0.86

[a] The pressure dependence of the quantum yield was measured relative to the value at 60 Torr using a 532 nm cavity ring-down probe wavelength and constant photolyte concentration and photolysis laser fluence as described in the text; $[CH_3C(O)CH_3] = 5.15 \times 10^{15}$ molecule cm^{-3}, $[CH_3C(O)C(O)CH_3] = 5.22 \times 10^{15}$ molecule cm^{-3}, $[CH_3C(O)CH_2CH_3] = 5.35 \times 10^{15}$ molecule cm^{-3}. Quantum yields at pressures >60 Torr in the acetone experiments are the average from 3 separate measurements. The precision of these measurements was ~5%. The quantum yields at pressures >60 Torr for biacetyl and methyl ethyl ketone were obtained from a single sequence of measurements. The absolute uncertainty in the quantum yields is ±15%, 2σ confidence level, and includes estimated systematic errors (see Section 3.1 for details).

Table 3
Summary of CH_3CO quantum yield results in the 248 nm photolysis of acetone, biacetyl and methyl ethyl ketone with He bath gas from this work at 296 K[a]

Acetone ($CH_3C(O)CH_3$)		Biacetyl ($CH_3C(O)C(O)CH_3$)		Methyl ethyl ketone ($CH_3C(O)CH_2CH_3$)	
Pressure (Torr)	Quantum yield	Pressure (Torr)	Quantum yield	Pressure (Torr)	Quantum yield
62	0.60	60	0.76	60	0.51
108	0.62	109	0.79	114	0.54
210	0.70	204	0.78	205	0.55
314	0.71	306	0.81	353	0.60
408	0.73	404	0.84	495	0.65
506	0.76	516	0.82	669	0.65
603	0.78	606	0.81	–	–
604	0.79	671	0.85	–	–
670	0.82	–	–	–	–

[a] The pressure dependence of the quantum yield was measured relative to the value at 60 Torr using a 532 nm cavity ring-down probe wavelength and constant photolyte concentration and photolysis laser fluence as described in the text; $[CH_3C(O)CH_3] = 5.36 \times 10^{15}$ molecule cm^{-3}, $[CH_3C(O)C(O)CH_3] = 5.26 \times 10^{15}$ molecule cm^{-3}, $[CH_3C(O)CH_2CH_3] = 5.24 \times 10^{15}$ molecule cm^{-3}. The quantum yields at pressures >60 Torr were obtained from a single sequence of measurements. The absolute uncertainty in the quantum yields is ±15%, 2σ confidence level, and includes estimated systematic errors (see Section 3.1 for details).

where only the total pressure of the system was changed, i.e., the laser fluence and photolyte concentration were nearly constant. This approach greatly improved the precision of the determination of the pressure dependence in Φ_{CH_3CO}. A systematic increase in Φ_{CH_3CO} with increasing bath gas pressure was observed for each of the ketones and the observed pressure dependence was larger with N_2 than with He as the bath gas.

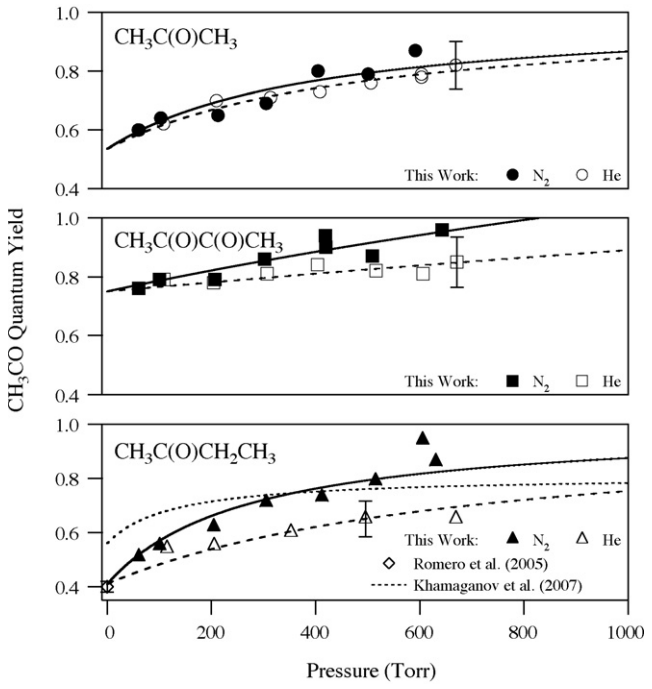

Fig. 4. The CH_3CO quantum yield at 296 K following the 248 nm pulsed laser photolysis of acetone (CH_3COCH_3), biacetyl ($CH_3C(O)C(O)CH_3$), and methyl ethyl ketone ($CH_3C(O)CH_2CH_3$) dependence on bath gas collision partner (He (open symbols, dashed lines), N_2 (solid symbols and lines)) and total bath gas pressure. The curves are fits of the data to Eq. (21) and the parameters obtained are given in Table 4. For comparison with our methyl ethyl ketone results, the CH_3CO low pressure quantum yield reported by Romero et al. [27] (◊) and the results from a Stern–Volmer analysis from Khamaganov et al. [13] (dotted line) are included.

In the 248 nm photolysis of acetone, nascent CH_3CO is produced with sufficient internal energy, 30.6 kcal mol^{-1}, for it to decompose into CH_3 + CO [12,13,24]

$$CH_3C(O)CH_3 + h\nu \rightarrow CH_3CO^* + CH_3 \quad (18)$$

$$CH_3CO^* + M \rightarrow CH_3CO + M \quad (19)$$

$$CH_3CO^* \rightarrow CH_3 + CO \quad (20)$$

where CH_3CO^* represents an activated CH_3CO molecule that is formed with sufficient internal energy to dissociate. Similar photolysis schemes can be written for MEK and biacetyl although the energy available for activation of CH_3CO is slightly different (34.5 kcal mol^{-1} for biacetyl and 31.7 kcal mol^{-1} for MEK). The minimum energy needed to thermally dissociate CH_3CO is ~16 kcal mol^{-1}, 11 kcal mol^{-1} in zero-point energy and ~5 kcal mol^{-1} to overcome a barrier in the dissociation exit channel. This simplified mechanism is consistent with the more detailed theoretical treatment given by Somnitz et al. [12] for the dissociation of CH_3CO following the photodissociation of acetone. On the basis of molecular beam photofragment translational spectroscopy measurements, North et al. [24] determined that ~30% of the initially formed CH_3CO contains sufficient internal energy to dissociate. This is consistent with our Φ_{CH_3CO} value of 0.60 measured at 60 Torr.

The observed pressure dependence is reproduced reasonably well, over the range of pressures covered in this study, by a Stern–Volmer relationship for the formation of CH_3CO from CH_3CO^*

$$\Phi_{CH_3CO} = \Phi^0_{CH_3CO} + (\Phi^\infty_{CH_3CO} - \Phi^0_{CH_3CO}) \times \left(\frac{k_{19}[M]}{k_{19}[M] + k_{20}}\right) \quad (21)$$

where $\Phi^0_{CH_3CO}$ is the quantum yield in the zero pressure limit, $\Phi^\infty_{CH_3CO}$ is the quantum yield in the high pressure limit, and M is the bath gas number density in molecule cm^{-3}. Fits of the experimental data were performed using $\Phi^\infty_{CH_3CO}$ values of 1 for acetone and MEK and 2 for biacetyl. This approximation is reasonable for acetone and MEK, although the true value of $\Phi^\infty_{CH_3CO}$ may be slightly less than 1, but most likely is an over-estimate for biacetyl. Therefore, this analysis is only valid over the range of pressures used in the present measurements. Additional quantum yield data for biacetyl photolysis at pressures higher than used in the present study are needed to refine the analysis further. The results of the fits are shown in Fig. 4 and given in Table 4. For acetone, the fit yields k_{19}/k_{20} of $(0.6 \pm 0.2) \times 10^{-19}$ cm^3 molecule^{-1} for He and $(0.8 \pm 0.2) \times 10^{-19}$ cm^3 molecule^{-1} for N_2 bath gas. Assuming $k_{19} = 1 \times 10^{-12}$ cm^3 molecule^{-1} s^{-1}, a reasonable rate coefficient for the collisional quenching of CH_3CO^*, then $k_{20} \approx 1.4 \times 10^7$ s^{-1}, a lifetime of <100 ns for the activated CH_3CO^* radical. Therefore, the activated CH_3CO^* radical is short-lived. Our estimated CH_3CO^* lifetime is consistent with values estimated by Somnitz et al. [12] and Khamaganov et al. [13].

At the highest pressures used in this study, the CH_3CO quantum yield in the photolysis of acetone approaches unity. This implies that channel (1b), which produces $2CH_3$ + CO as primary photolysis products, has a small yield, <10%, and that the CO produced in the 248 nm photolysis of acetone is primarily via the decomposition of activated CH_3CO. The present work shows that acetone photolysis at 248 nm always leads to dissociation. However, the activated CH_3CO dissociates unless it is stabilized, which accounts for the pressure dependence of Φ_{CH_3CO}.

It is worth pointing out that although the available energy for nascent CH_3CO radical excitation in the photolysis of acetone, MEK and biacetyl are similar, the measured pressure and collision partner dependences in Φ_{CH_3CO} are different as shown in Fig. 4 and given in Table 4. For example, the pressure dependence observed in

Table 4
Results from a Stern–Volmer analysis $\Phi_{CH_3CO} = \Phi^0_{CH_3CO} + (\Phi^\infty_{CH_3CO} - \Phi^0_{CH_3CO}) \times (k_{19}[M]/(k_{19}[M] + k_{20}))$ of the CH_3CO quantum yield pressure dependence in the 248 nm photolysis of acetone ($CH_3C(O)CH_3$), methyl ethyl ketone ($CH_3C(O)CH_2CH_3$), and biacetyl ($CH_3C(O)C(O)CH_3$) at 296 K[a]

Photolyte	$\Phi^0_{CH_3CO}$	$\Phi^\infty_{CH_3CO}$	k_{19}/k_{20} (10^{-19} cm^3 molecule^{-1})		Reference
			N_2	He	
$CH_3C(O)CH_3$	0.535 ± 0.06[b]	1[c]	0.8 ± 0.2	0.6 ± 0.2	This work
	0.58 ± 0.06	1	1.2 ± 0.3	–	Khamaganov et al. [13]
$CH_3C(O)CH_2CH_3$	0.41 ± 0.05	1[c]	1.1 ± 0.3	0.43 ± 0.12	This work
	0.56 ± 0.1	0.81 ± 0.03	2.5 ± 0.8	–	Khamaganov et al. [13]
$CH_3C(O)C(O)CH_3$	0.76 ± 0.05	2[c]	0.09 ± 0.02	0.04 ± 0.01	This work

[a] $\Phi^0_{CH_3CO}$ is the quantum yield in the low-pressure limit, $\Phi^\infty_{CH_3CO}$ is the quantum yield in the high pressure limit, and M is the bath gas number density in molecule cm^{-3}. The $\Phi^\infty_{CH_3CO}$ values were fixed to the values given in the table in the analysis.

[b] $\Phi^0_{CH_3CO}$ values are an average of the values obtained from separate fits of the N_2 and He data. The uncertainties quoted for this work are 1σ from the precision of the least-squares fits.

[c] Fixed in the Stern–Volmer analysis.

the CH_3CO quantum yield for biacetyl is significantly greater than that determined for either acetone or MEK.

3.1. Error analysis

The absolute uncertainty in Φ_{CH_3CO} was determined from the uncertainties in the parameters used in Eq. (10). Using the relative quantum yield method minimizes uncertainties due to the measurement parameters such as laser fluence, absorption pathlength, gas flow, and pressure, which are kept nearly constant during an experiment. Therefore, uncertainties in these parameters make only a small contribution to the overall uncertainty in Φ_{CH_3CO}. The measured CRDS time constant measurements were relatively accurate, ±1%. The linearity of CH_3CO radical production was confirmed experimentally, ±5%, as shown in Figs. 2 and 3, over the same range of concentrations and laser fluences used in our quantum yield determination. The precursor concentrations were measured online by UV absorption before and after the reactor and agreed to within 5%. In addition, the uncertainty in the precursor absorption cross-sections (Table 1), partially cancel in the data analysis; we estimate the uncertainty in the cross-sections to contribute ≤5%.

Different CRD probe wavelengths and two separate OH radical sources were used in the determination of Φ_{CH_3CO}. Φ_{CH_3CO} values obtained using the different OH sources agreed to within 10% (also see Rajakumar et al. [15]). Measurements made using different probe wavelengths agreed to within 10%. The agreement of the quantum yields obtained using different CRDS probe wavelengths is best illustrated by the consistency of the CH_3CO visible absorption spectra obtained using 248 nm photolysis of acetone, MEK, and biacetyl as given in Rajakumar et al. [15]. By combining the above uncertainties, we estimate the overall uncertainty in Φ_{CH_3CO} from acetone, MEK, and biacetyl photolysis at 248 nm to be 15% at the 2σ (95% confidence) level. The estimated uncertainty encompasses the full range of Φ_{CH_3CO} values measured during the course of this study.

3.2. Previous quantum yield studies

The scope of our discussion of previous quantum yield studies presented here is limited to a comparison of our results with several of the most recent studies of the photolysis of acetone, MEK, and biacetyl [1,5,7,8,12,13,25–27]. As mentioned in the Introduction of this paper, the 248 nm acetone quantum yield has been shown previously to be near unity and independent of pressure, i.e., fluorescence and quenching are minor loss processes compared to dissociation [5,6]. However, some discrepancies exist for the quantum yield branching ratio and the pressure dependence that are discussed here.

Our CH_3CO quantum yields in the 248 nm photolysis of acetone can be compared with values recently reported by Khamaganov et al. [13] and the University of Leeds group [1,7,27]. In addition, we will compare our results with the CO quantum yields reported by Somnitz et al. [12]. Khamaganov et al. [13] reported quantum yields for the CH_3CO and CH_3 radicals at total pressures over the range 5–1500 Torr (N_2). Radical formation was measured following the pulsed laser photolysis of acetone at 248 nm by monitoring the transient UV absorption of the CH_3 radical (CH_3I photolysis was used as a reference calibration source for CH_3 radicals) CH_3CO quantum yields were also determined using transient UV absorption, although the accuracy of these measurements was lower than for CH_3. Khamaganov et al. report a negative pressure dependence for Φ_{CH_3} that is reproduced by the empirical formula $\Phi_{CH_3} = 1 + 0.45 \times \exp[-0.002 \times P]$, where P is the total pressure of N_2 in Torr. The corresponding positive pressure dependence in Φ_{CH_3CO}, given by $2 - \Phi_{CH_3}$, is greater than their measured Φ_{CH_3CO} but yields a value at 60 Torr (N_2) of 0.60 ± 0.06 in good agreement with the results from our study. In addition, the pressure dependence of Φ_{CH_3CO} (inferred from their Φ_{CH_3} measurements) is in good agreement with our measured pressure dependence. The Stern–Volmer analysis results from the Khamaganov et al. [13] study are included in Fig. 5 for comparison with this work.

The Leeds group has reported Φ_{CH_3CO} values for the 248 nm photolysis of acetone that fall in the range 0.35–0.40 in the low-pressure limit (He bath gas) [1,7,27]. These CH_3CO quantum yield values are significantly smaller than the low-pressure value obtained in our study. In the Leeds studies, CH_3CO radical formation was monitored by the detection of OH radicals formed as a product in the $CH_3CO + O_2 + M$ reaction. Φ_{CH_3CO} was determined relative to CH_3CO quantum yield measurements made at longer photolysis wavelengths, 310 and 320 nm, where the CH_3CO quantum yield at low pressure is assumed to be unity. It was also assumed in their data analysis that Φ_{CH_3CO} for the 248 nm photolysis of acetone was independent of pressure, contrary to results from this study and the results of Khamaganov et al. [13] and Somnitz et al. [12] (discussed below). Including a pressure dependence in the data analysis of the Leeds work will directly impact the acetone photolysis quantum yields obtained at longer wavelengths, >300 nm, from their work.

Somnitz et al. [12] reported Φ_{CO} for acetone photolysis at 248 nm at pressures over the range 20–900 Torr (N_2). Quantum yields were determined by monitoring the formation of CO, using infrared diode laser absorption of CO, following the exposure of acetone/N_2 samples to a small number, <100, of 248 nm photolysis laser pulses. Multiple photolysis laser pulses were needed to build up [CO] to measurable levels. Φ_{CO} values between 0.45 at 20 Torr and 0.25 at 900 Torr were reported, see Fig. 5. At low pressure, the CO quantum yield results are in good agreement with the CH_3CO quantum

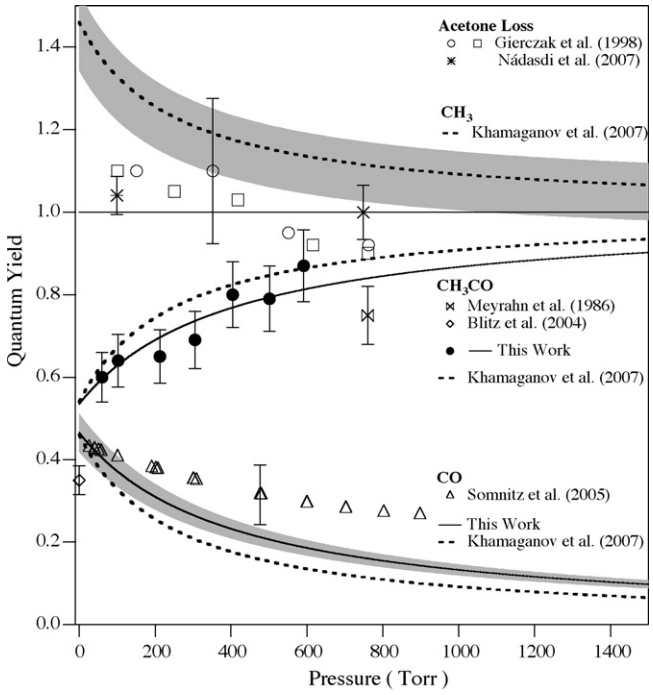

Fig. 5. Comparison of the CH_3CO quantum yields in the 248 nm photolysis of acetone measured in this work with N_2 bath gas (●, solid line (Stern–Volmer fit, Eq. (21))) with results from previous studies. The error bars for the data from this work are at the 2σ level and include estimated systematic errors. The error bars for the literature data are as reported. Previous studies include: acetone loss (○, syn. air bath gas) and CO_2 formation quantum yields (□, syn. air bath gas) from Gierczak et al. (1998) [5]; acetone loss (∗, syn. air bath gas) from Nádasdi et al. (2007) [6]; the CH_3CO quantum yield from the Leeds group [1,7,27] (◊, He bath gas) and Meyrahn et al. [25] (bowtie, syn. air bath gas); the CO quantum yield pressure dependence from Somnitz et al. (2005) [12] (△, N_2 bath gas); the CH_3 quantum yield pressure dependence reported by Khamaganov et al. (2007) [13] obtained from a Stern–Volmer analysis, $\Phi_{CH_3} = 0.46 \times (1 + 4 \times 10^{-3} \times P)^{-1} + 1$ (dashed line), and the corresponding CH_3CO and CO quantum yields calculated using these fit parameters, $\Phi_{CH_3CO} = 2 - \Phi_{CH_3}$ and $\Phi_{CO} = 1 - \Phi_{CH_3CO}$. The shaded areas represent estimated uncertainties.

yields obtained in this work and a unit acetone quantum yield [5,6]. However, there is a systematic discrepancy in the reported pressure dependence in Φ_{CO} and our results with the decrease in Φ_{CO} reported by Somnitz et al. being smaller than the increase in Φ_{CH_3CO} obtained in our work.

There are two frequently referenced acetone photolysis end-product studies that need to be included in this discussion. Meyrahn et al. [25] reported $\Phi_{CH_3CO} = 0.75 \pm 0.07$ for the 250 nm photolysis of acetone at 760 Torr (syn. air). In their study, Φ_{CH_3CO} was determined using quantitative measurements of $CH_3C(O)OONO_2$ (PAN) produced by the addition of NO_2 to the mixture, reactions (2) and (3). Although end-product studies in general, are susceptible to possible systematic error as a result of unwanted gas-phase radical chemistry, their Φ_{CH_3CO} value is in reasonable agreement with our results, although somewhat lower, near atmospheric pressure (see Fig. 5). Second, in a previous study from our laboratory, Gierczak et al. [5] reported the CO_2 photolysis yield in the 248 nm photolysis of acetone in synthetic air to be near unity, 1.0 ± 0.15, and independent of pressure within the precision of the measurements. The formation of CO_2 as an end-product was attributed solely to the formation of CH_3CO radicals as a primary acetone photolysis product. This interpretation is not consistent with the present results unless the collisional stabilization of the activated CH_3CO radicals by O_2 is much more efficient than N_2. Unfortunately, the O_2 collisional stabilization efficiency could not be measured in the present work due to the rapid loss of CH_3CO via reaction (2).

The photochemistry of MEK and biacetyl has received much less attention than acetone. Khamaganov et al. [13] and Romero et al. [27] have reported Φ_{CH_3} and Φ_{CH_3CO} values, for MEK, respectively, following 248 nm pulsed laser photolysis. For comparison purposes, the CH_3CO quantum yields reported in the Khamaganov et al. and Romero et al. studies are included in Fig. 4. Khamaganov et al. reported a Stern–Volmer analysis for their measured pressure dependence of the CH_3 radical quantum yield (see Table 4). Their analysis yields $\Phi^0_{CH_3CO} = 0.56$ which is significantly greater than obtained in our work. The source of this discrepancy is currently unknown. Romero et al. [27] reported $\Phi^0_{CH_3CO} = 0.40 \pm 0.02$ and estimated the quantum yield of the CH_3CH_2O radical to be <0.18. The $\Phi^0_{CH_3CO}$ value obtained in our work is in reasonable agreement, within the combined 2σ uncertainty limits, with the value reported by Romero et al. In addition to the studies of primary photolysis products, it is also worth mentioning the broadband MEK photolysis study of Raber and Moortgat [28]. They report measurements of MEK photodissociation for wavelengths >275 nm using fluorescent photolysis lamps. The loss of MEK and formation of stable end-products was measured by infrared absorption. They report "effective" pressure dependent MEK quantum yields where $\Phi^{-1}_{MEK} = 1 + 2.22 \times 10^{-3} \times P$ (where P is in Torr of syn. air). Direct measurements of Φ_{CH_3CO} for MEK at wavelengths >290 nm are, however, still needed for input into atmospheric model calculations.

To the best of our knowledge, there are no measurements of Φ_{CH_3CO} at 248 nm for biacetyl currently available in the literature. Previous biacetyl photochemical studies have focused on the determination of effective atmospheric photolysis rates [29] rather than specific primary photolysis product identification and its wavelength dependence. In their study, Klotz et al. [29] pointed out the need for wavelength dependent quantum yield measurements to refine atmospheric photochemical mechanisms.

4. Summary

We have measured CH_3CO quantum yields following the 248 nm pulsed laser photolysis of acetone, MEK, and biacetyl over the pressure range 60–670 Torr with He and N_2 bath gases. The observed dependence of Φ_{CH_3CO} on pressure and bath gas implies that a fraction of the nascent CH_3CO primary photolysis product is energetically activated and dissociate to $CH_3 + CO$ prior to collisional stabilization. For acetone, the CH_3CO quantum yield, channel (1b), approaches unity at high pressure implying that the CO radical is not a significant primary photolysis product at 248 nm. The CH_3CO quantum yields for the 248 nm photolysis of methyl ethyl ketone and biacetyl also show a positive pressure dependence, however, for these molecules other photolysis channels may also be significant. Measurements of the CO quantum yield in the 248 nm photolysis of methyl ethyl ketone and biacetyl would be useful for quantifying the branching ratios of the various photolysis channels.

Acknowledgements

This work was supported in part by NOAA's Climate Change program and NASA's Atmospheric Composition Program.

References

[1] M.A. Blitz, D.E. Heard, M.J. Pilling, J. Phys. Chem. A 110 (2006) 6742–6756.
[2] S.A. McKeen, T. Gierczak, J.B. Burkholder, P.O. Wennberg, T.F. Hanisco, E.R. Keim, R.-S. Gao, S.C. Liu, A.R. Ravishankara, D.W. Fahey, Geophys. Res. Lett. 24 (1997) 3177–3180.
[3] S.P. Sander, R.R. Friedl, D.M. Golden, M.J. Kurylo, G.K. Moortgat, P.H. Wine, A.R. Ravishankara, C.E. Kolb, M.J. Molina, B.J. Finlayson-Pitts, R.E. Huie, V.L. Orkin,

Chemical Kinetics and Photochemical Data for Use in Atmospheric Studies, JPL Pub. 06-2, Jet Propulsion Laboratory, Pasadena, 2006.
[4] NIST Chemistry WebBook, NIST Standard Reference Database Number 69, June 2005 Release, http://webbook.nist.gov/chemistry/.
[5] T. Gierczak, J.B. Burkholder, S. Bauerle, A.R. Ravishankara, Chem. Phys. 231 (1998) 229–244.
[6] R. Nádasdi, G. Kovács, I. Szilágyi, A. Demeter, S. Dóbé, T. Bérces, F. Márta, Chem. Phys. Lett. 440 (2007) 31–35.
[7] M.A. Blitz, D.E. Heard, M.J. Pilling, S.R. Arnold, M.P. Chipperfield, Geophys. Res. Lett. 31 (2004) L06111.
[8] M. Emrich, P. Warneck, J. Phys. Chem. A 104 (2000) 9436–9442.
[9] A. Horowitz, J. Phys. Chem. 95 (1991) 10816–10823.
[10] E.P. Gardner, R.D. Wijayaratne, J.G. Calvert, J. Phys. Chem. 88 (1984) 5069–5076.
[11] P.D. Lightfoot, S.P. Kirwan, M.J. Pilling, J. Phys. Chem. 92 (1988) 4938–4946.
[12] H. Somnitz, M. Fida, T. Ufer, R. Zellner, Phys. Chem. Chem. Phys. 7 (2005) 3342–3352.
[13] V. Khamaganov, R. Karunanandan, A. Rodriguez, J.N. Crowley, Phys. Chem. Chem. Phys. 9 (2007) 4098–4113.
[14] M.C. Thurber, R.K. Hanson, App. Phys. B: Lasers Opt. 69 (1999) 229–240.
[15] B. Rajakumar, J.E. Flad, T. Gierczak, A.R. Ravishankara, J.B. Burkholder, J. Phys. Chem. A 111 (2007) 8950–8958.
[16] N.I. Butkovskaya, A. Kukui, G. Le Bras, J. Phys. Chem. A 108 (2004) 1160–1168.
[17] M. Cameron, V. Sivkumaran, T.J. Dillon, J.N. Crowley, Phys. Chem. Chem. Phys. 4 (2002) 3628–3638.
[18] S.S. Brown, A.R. Ravishankara, H. Stark, J. Phys. Chem. A 104 (2000) 7044–7052.
[19] S.S. Brown, R.W. Wilson, A.R. Ravishankara, J. Phys. Chem. A 104 (2000) 4976–4983.
[20] J.E. Flad, S.S. Brown, J.B. Burkholder, H. Stark, A.R. Ravishankara, Phys. Chem. Chem. Phys. 8 (2006) 3636–3642.
[21] A. O'Keefe, D.A.G. Deacon, Rev. Sci. Inst. 59 (1988) 2544–2551.
[22] H. Adachi, N. Basco, D.G.L. James, Int. J. Chem. Kinet. 13 (1981).
[23] M.M. Maricq, J.J. Szente, Chem. Phys. Lett. 253 (1996) 333–339.
[24] S.W. North, D.A. Blank, J.D. Gezelter, C.A. Longfellow, Y.T. Lee, J. Chem. Phys. 102 (1995) 4447–4460.
[25] H. Meyrahn, J. Pauly, W. Schneider, P. Warneck, J. Atmos. Chem. 4 (1986) 277–291.
[26] M. Emrich, P. Warneck, J. Phys. Chem. A 109 (2005) 1752.
[27] M.T.B. Romero, M.A. Blitz, D.E. Heard, M.J. Pilling, B. Price, P.W. Seakins, L. Wang, Faraday Discuss. 130 (2005) 73–88, doi:10.1039/b419160a.
[28] W.H. Raber, G.K. Moortgat, in: J.R. Barker (Ed.), Problems and Progress in Atmospheric Chemistry, World Scientific, 2000, pp. 318–373.
[29] B. Klotz, F. Graedler, S. Sorensen, I. Barnes, K.H. Becker, Int. J. Chem. Kinet. 33 (2001) 9–20.
[30] J.B. Burkholder, R.K. Talukdar, Geophys. Res. Lett. 21 (1994) 581–584.
[31] R.D. Martinez, A.A. Buitrago, N.W. Howell, C.H. Hearn, J.A. Joens, Atmos. Environ. 26A (1992) 785–792.
[32] A. Horowitz, R. Meller, G.K. Moortgat, J. Photochem. Photobiol. A: Chem. 146 (2001) 19–27.